

Bifurcation of elastic curves with modulated stiffness

Katharina Brazda¹, Gaspard Jankowiak², Christian Schmeiser¹, Ulisse Stefanelli^{1,3,4}

¹University of Vienna, Faculty of Mathematics, Oskar-Morgenstern-Platz 1, 1090 Wien, Austria

²Radon Institute for Applied and Computational Mathematics, Altenbergerstr. 69, 4040, Linz, Austria

³Vienna Research Platform on Accelerating Photoreaction Discovery, University of Vienna, Währingerstraße 17, 1090 Wien, Austria

⁴Istituto di Matematica Applicata e Tecnologie Informatiche E. Magenes, via Ferrata 1, I-27100 Pavia, Italy

October 14, 2021

Abstract

We investigate the equilibrium configurations of closed planar elastic curves of fixed length, whose stiffness, also known as the bending rigidity, depends on an additional density variable. The underlying variational model relies on the minimization of a bending energy with respect to shape and density and can be considered as a one-dimensional analogue of the Canham-Helfrich model for heterogeneous biological membranes. We present a generalized Euler-Bernoulli elastica functional featuring a density-dependent stiffness coefficient. In order to treat the inherent nonconvexity of the problem we introduce an additional length scale in the model by means of a density gradient term. We derive the system of Euler-Lagrange equations and study the bifurcation structure of solutions with respect to the model parameters. Both analytical and numerical results are presented.

MSC 2020: 35J20, 35B38, 35B32, 35B36, 74G65, 74K10

Keywords: Canham-Helfrich energy, elastic curves, energy minimization, stationary points, pitchfork bifurcation

Contents

1	Introduction	2
2	Mathematical setting	3
2.1	Notation and preliminaries on curves	3
2.2	Elastic energies with modulated stiffness	4
3	Existence and nonexistence	5
4	Bifurcation analysis	9
4.1	Euler-Lagrange equations	9
4.2	Linearization around the trivial state	9
4.3	Asymptotic expansion around bifurcation points	12
4.4	Energy and stability	14
5	Numerical continuation of bifurcation branches	15
5.1	Discretization	15
5.2	Choice of parameters	16
5.3	Results	17

1 Introduction

We investigate the equilibrium configurations of elastic curves featuring an additional scalar density variable which influences the bending rigidity. Our interest is motivated by the variational modelization of the *shapes of biological membranes*, originally proposed by CANHAM [6] and HELFRICH [15] to explain the characteristic biconcave shape of a human red blood cell. According to this model, the equilibrium membrane shape Σ minimizes the bending energy

$$E_{\text{CH}}(\Sigma) = \int_{\Sigma} \left(\frac{\beta}{2} (H - H_0)^2 + \gamma K \right) dS$$

under suitable constraints on membrane area and enclosed volume. Here, Σ is a smooth closed surface embedded in \mathbb{R}^3 , H and K are the mean and the Gauss curvature of Σ , respectively, and the material parameters comprise the stiffnesses (bending rigidities) $\beta > 0$, $\gamma < 0$ as well as the spontaneous curvature $H_0 \in \mathbb{R}$. The material parameters of heterogeneous biomembranes are assumed to depend on the variable membrane composition, which is described by a scalar function $\rho: \Sigma \rightarrow \mathbb{R}$ which we interpret as a density of fixed total mass. On the other hand, the geometry of the membrane influences the distribution of the density ρ , which originates a *coupling effect between curvature and composition*. Indeed, the energy for heterogeneous biomembranes has to be minimized with respect to both membrane geometry Σ and composition ρ simultaneously. Configurations featuring this coupling have been experimentally observed for example by BAUMGART, HESS, & WEBB [3] in case of giant unilamellar vesicles. Furthermore, the coupling effect also plays an essential role in the dynamic morphology changes of cells, where special curved membrane proteins are involved, cf. McMAHON & GALLOP [21].

Results on the mathematical analysis of the variational problem for heterogeneous biomembranes have been obtained by CHOKSI, MORANDOTTI, & VENERONI [7] and HELMERS [17], who proved the existence of multiphase minimizers in the axisymmetric regime. By dropping the symmetry restriction, existence of multiphase minimizers has been recently obtained by [5] in the weak setting of *varifolds*. For a collection of recent results on both single- and multiphase Canham-Helfrich models the reader is referred to [2, 5, 10, 12, 13, 19, 22, 24, 26].

To the best of our knowledge, proving existence of minimizers for membranes featuring continuous phase densities and general material parameter models is an open problem. We move a first step in this direction in the present paper, by focusing on the lower-dimensional setting of curves instead. A classical elastic curve in the plane, $\gamma: [0, L] \rightarrow \mathbb{R}^2$, minimizes the EULER-BERNOULLI elastic bending energy (also known as the WILLMORE energy)

$$E(\gamma) = \frac{1}{2} \int_{\gamma} \kappa^2 ds,$$

where κ is the scalar curvature of γ . The stationary points are called *elasticae* and can be analytically described in terms of elliptic functions. As was already clear to Euler, the only closed elasticae of fixed length in the plane are the circle and Bernoulli's Figure-8 curve, the single covered circle being the unique global minimizer of E , see for example TRUESDELL [25] and LANGER & SINGER [18].

We now modify the setting by taking the additional scalar density ρ into the picture. The density ρ modulates the elastic behavior of the curve. For this purpose we consider the following elastic bending energy with *density-modulated stiffness*,

$$E_0(\rho, \gamma) = \frac{1}{2} \int_{\gamma} \beta(\rho) \kappa^2 ds.$$

Our interest lies on the effects of the variable stiffness β and we dispense with the spontaneous curvature H_0 , for simplicity. In order to take into account the coupling between shape and composition, we have to minimize E_0 with respect to both γ and ρ . Admissible curves γ are asked to be planar, regular, C^1 -closed, and have fixed length L , whereas admissible densities ρ are required to have fixed mass $\int_{\gamma} \rho ds = M$.

The application of the Direct Method for the minimization of E_0 calls for checking lower semicontinuity with respect to weak topologies, which in turn asks for the convexity of the integrand of E_0 . Yet, if such convexity is imposed, only the trivial minimizer exists, namely the constant density $\rho_0 = M/L$ on a circle with curvature $\kappa_0 = 2\pi/L$. This however is insufficient for describing the rich geometric morphologies that can be observed in biological membranes.

In the following, we will therefore not assume convexity of the integrand of E_0 . This lack of convexity may however lead to nonexistence of minimizers, see Section 3 below. We are hence forced to consider a regularized energy E_μ , featuring an additional length scale in terms of a gradient term in ρ , namely,

$$E_\mu(\rho, \gamma) = \frac{1}{2} \int_\gamma (\beta(\rho) \kappa^2 + \mu \dot{\rho}^2) ds, \quad (1.1)$$

where $\dot{\rho} := \frac{d}{ds} \rho$. The parameter μ may be physically interpreted as the diffusivity of the density, cf. (2.5). For μ large, the only minimizer is the trivial one, see Proposition 3.3. By lowering μ one observes the onset of bifurcations from the trivial state. The main focus of this paper is the rigorous bifurcation analysis in terms of μ . We analytically classify the bifurcation behavior of solutions of the Euler-Lagrange equations of E_μ . Moreover, we provide an exhaustive suite of numerical experiments, illustrating the distinguished patterning of minimizers of E_μ , depending on μ .

A variational model for planar elastic curves with density has also been studied by HELMERS [16]. He focused on the effect of spontaneous curvature and established a Γ -convergence result to the sharp interface limit. Let us mention also the recent work by PALMER & PÁMPANO [23], who presented analysis and numerics for the shapes of elastic rods with anisotropic bending energies.

We conclude this introduction by presenting the outline of the paper. In Section 2, we briefly describe the mathematical setting and explain our notation. Section 3 is devoted to the justification of our model by existence and nonexistence results for minimizers. In Section 4 we analytically discuss the local bifurcation structure of solutions to the associated Euler-Lagrange equations. Numerical results for the bifurcation branches as well as for the configurations of the curves are presented in Section 5. Finally, Section 6 summarizes our findings.

2 Mathematical setting

We devote this section to make the mathematical setting precise and fix notation.

2.1 Notation and preliminaries on curves

We collect some basic information on curves [11]. In the following, we will consider *closed planar curves* $\gamma \in H^2(\mathbb{T}_L)^2$, where $\mathbb{T}_L := \mathbb{R}/L\mathbb{Z}$ is the one-dimensional torus with period $L > 0$. The fact that $H^2(\mathbb{T}_L) \subset C^1(\mathbb{T}_L)$ ensures that $\gamma: [0, L] \rightarrow \mathbb{R}^2$ represents a C^1 -closed curve and $\gamma(0) = \gamma(L)$ and $\dot{\gamma}(0) = \dot{\gamma}(L)$. We systematically assume γ to be parametrized by arc-length s , namely, $|\dot{\gamma}| = 1$. This induces that $\ddot{\gamma} \in L^2(\mathbb{T}_L)^2$ is orthogonal to $\dot{\gamma}$. The normal vector n to the curve is defined pointwise by counterclockwise rotating $\dot{\gamma}$ by $\pi/2$. That is, by denoting $\gamma(s) = (x(s), y(s))$, $n(s) = \dot{\gamma}(s)^\perp := (-\dot{y}(s), \dot{x}(s))$. The rate of change of $\dot{\gamma}$ in direction n is measured by the scalar *curvature* $\kappa = n \cdot \ddot{\gamma} = \det(\dot{\gamma}, \ddot{\gamma}) \in L^2(\mathbb{T}_L)$ of the curve, so that $\ddot{\gamma} = (n \cdot \ddot{\gamma}) n = \kappa n$.

The *inclination angle* $\theta \in L^2(\mathbb{T}_L)$ is the angle between the x -axis and the tangent $\dot{\gamma}$, that is $\dot{\gamma} = (\dot{x}, \dot{y}) = (\cos \theta, \sin \theta)$. Note that in even for smooth γ , θ is discontinuous on \mathbb{T}_L . However, the map $s \mapsto \theta(s) - \frac{2\pi}{L} I s$ is an element of $H^1(\mathbb{T}_L)$, where the *rotation index* of the curve $I \in \mathbb{Z}$ counts the number of complete turns of $\dot{\gamma}$ according to the standard orientation, see below. The curvature function $\kappa \in L^2(\mathbb{T}_L)$ uniquely determines the curve $\gamma \in H^2(\mathbb{T}_L)^2$ up to translations and rotations in \mathbb{R}^2 [11, Section 1-5, pp. 19, 24, and Section 1-7, p. 36]. In particular, if $|\dot{\gamma}| = 1$, then

$$\kappa = \dot{\theta}, \quad \theta(s') = \theta(0) + \int_0^{s'} \kappa(s'') ds'', \quad \text{and} \quad \gamma(s) = \begin{pmatrix} x(s) \\ y(s) \end{pmatrix} = \begin{pmatrix} x(0) \\ y(0) \end{pmatrix} + \int_0^s \begin{pmatrix} \cos \theta(s') \\ \sin \theta(s') \end{pmatrix} ds'. \quad (2.1)$$

Identifying all curves whose images only differ by isometries in \mathbb{R}^2 , one may adapt the coordinate system to $x(0) = y(0) = \theta(0) = 0$, corresponding indeed to the choice $\gamma(0) = (0, 0)$ and $\dot{\gamma}(0) = (1, 0)$. A curve $\gamma \in H^2(\mathbb{T}_L)^2$ parametrized by arc-length satisfies the following identities:

$$\begin{aligned} 0 = \gamma(L) - \gamma(0) &= \int_0^L \dot{\gamma}(s) ds = \int_0^L \begin{pmatrix} \cos \theta(s) \\ \sin \theta(s) \end{pmatrix} ds = \int_0^L \begin{pmatrix} \cos \left(\theta(0) + \int_0^s \kappa(t) dt \right) \\ \sin \left(\theta(0) + \int_0^s \kappa(t) dt \right) \end{pmatrix} ds, \\ 0 = \dot{\gamma}(L) - \dot{\gamma}(0) &= (\cos \theta(L) - \cos \theta(0), \sin \theta(L) - \sin \theta(0)). \end{aligned}$$

The latter is equivalent to $\theta(L) - \theta(0) = \int_0^L \kappa(s) ds = 2\pi I$. A curve $\gamma: [0, L] \rightarrow \mathbb{R}^2$ is called *simple* if it is an injective map and *regular*, if it is C^1 and $\dot{\gamma}(t) \neq 0$ for all $t \in [0, L]$. By the Theorem of Turning Tangents [11,

Section 5-6, Theorem 2, p. 396], a simple C^1 -closed regular planar positively oriented C^1 curve has rotation index $I = 1$. This allows us to represent a simple C^1 -closed curve $\gamma \in H^2(\mathbb{T}_L)^2$ parametrized by arc-length by its inclination angle θ , granted that $\theta - \frac{2\pi}{L} I s \in H^1(\mathbb{T}_L)$ and

$$\theta(0) = 0, \quad \theta(L) = 2\pi \quad \text{and} \quad \int_0^L \begin{pmatrix} \cos \theta(s) \\ \sin \theta(s) \end{pmatrix} ds = 0,$$

or by its curvature $\kappa \in L^2(\mathbb{T}_L)$, additionally satisfying

$$\int_0^L \kappa(s) ds = 2\pi \quad \text{and} \quad \int_0^L \begin{pmatrix} \cos \left(\int_0^s \kappa(t) dt \right) \\ \sin \left(\int_0^s \kappa(t) dt \right) \end{pmatrix} ds = 0.$$

Eventually, note that by requiring a planar curve to be closed restricts the possible curvature functions. According to the Four Vertex Theorem [11, Section 1-7, Theorem 2, p. 37], a smooth simple closed regular planar curve has either constant curvature (i.e. is a circle) or the curvature function possesses at least four vertices, i.e. two local minima and two local maxima. The converse statement is given in [9]: every continuous function which either is a nonzero constant or has at least four vertices is the curvature of a simple closed regular planar curve.

2.2 Elastic energies with modulated stiffness

We consider planar curves $\gamma \in H^2(\mathbb{T}_L)^2$ parametrized by arc-length. With no loss of generality, we will assume from now on the length L of the curve to be 2π . The scalar density field $\rho: [0, 2\pi] \rightarrow \mathbb{R}$ is considered to be a function of the arc-length of the curve. Moreover, we are given a density-modulated stiffness

$$\beta \in C^2(\mathbb{R}) \quad \text{with} \quad \inf \beta =: \beta_m > 0. \quad (2.2)$$

In the following, we will assume (2.2) to hold throughout, without explicit mention. Note however that some results in this section are valid under weaker conditions on β as well.

Admissible curves are defined as elements of the set

$$\mathcal{A} := \left\{ \gamma \in H^2(\mathbb{T}_{2\pi})^2 : |\dot{\gamma}| = 1, \gamma(0) = \gamma(2\pi) = (0, 0), \dot{\gamma}(0) = \dot{\gamma}(2\pi) = (1, 0), \int_0^{2\pi} \det(\dot{\gamma}(s), \ddot{\gamma}(s)) ds = 2\pi \right\}.$$

In particular, admissible curves are planar, arc-length parametrized, and C^1 -closed. Note that we are not enforcing injectivity of γ (i.e. γ being simple) and we just require the weaker condition $I = 1$. This simplifies our tractation, having no effect on the bifurcation result (Section 4).

By the representation theorem for plane curves, any admissible curve $\gamma \in \mathcal{A}$ can be recovered from its inclination angle θ or its curvature κ . Correspondingly, we can equivalently indicate admissible curves as

$$\mathcal{A} = \left\{ \theta \in L^2(\mathbb{T}_{2\pi}) : \theta - s \in H^1(\mathbb{T}_{2\pi}), \int_0^{2\pi} \begin{pmatrix} \cos \theta(s) \\ \sin \theta(s) \end{pmatrix} ds = \begin{pmatrix} 0 \\ 0 \end{pmatrix}, \theta(0) = 0 \right\} \quad (2.3)$$

or

$$\mathcal{A} = \left\{ \kappa \in L^2(\mathbb{T}_{2\pi}) : \int_0^{2\pi} \begin{pmatrix} \cos \left(\int_0^s \kappa(t) dt \right) \\ \sin \left(\int_0^s \kappa(t) dt \right) \end{pmatrix} ds = \begin{pmatrix} 0 \\ 0 \end{pmatrix}, \int_0^{2\pi} \kappa(s) ds = 2\pi \right\}.$$

The abuse of notation in defining the set \mathcal{A} is motivated by the above-mentioned equivalence of the representations via γ , θ , and κ , up to fixing $\gamma(0) = (0, 0)$ and $\dot{\gamma}(0) = (1, 0)$ or $\theta(0) = 0$.

Admissible densities ρ are asked to have fixed total mass. By possibly redefining β , one may assume such mass to be 2π , which simplifies notation. Given the parameter $\mu \in [0, \infty)$, we define

$$\mathcal{P} := \left\{ \rho \in L^1(\mathbb{T}_{2\pi}) : \mu \rho \in H^1(\mathbb{T}_{2\pi}), \int_0^{2\pi} \rho(s) ds = 2\pi \right\}. \quad (2.4)$$

For the sake of simplicity, we do not restrict the values of ρ to be nonnegative, which would however be sensible, for ρ is interpreted as a density. Note however that this simplification has no effect on the bifurcation results, which are actually addressing a neighborhood of the trivial state only, where ρ is constant and positive.

The *elastic energy with modulated stiffness* is defined as

$$E_\mu(\rho, \gamma) := \int_0^{2\pi} \left(\frac{1}{2} \beta(\rho) \gamma^2 + \frac{\mu}{2} \rho^2 \right) ds. \quad (2.5)$$

Note that the energy E_μ can be equivalently rewritten as $E_\mu(\rho, \gamma) = E_\mu(\rho, \theta) = E_\mu(\rho, \kappa)$, again by abusing notation.

We identify elastic curves with modulated stiffness as minimizers of E_μ . In particular, we consider the following minimization problem

$$\boxed{\min_{(\rho, \gamma) \in \mathcal{P} \times \mathcal{A}} E_\mu(\rho, \gamma)}. \quad (2.6)$$

In contrast to the classical Euler-Bernoulli model for elasticae [18, 25], which is a purely geometric variational problem, here the density plays an active role in the selection of the optimal geometry.

3 Existence and nonexistence

As mentioned in the Introduction, the minimization of E_0 turns out to be of limited interest. Indeed, if the integrand

$$\Phi(\rho, \kappa) = \frac{1}{2} \beta(\rho) \kappa^2$$

is strictly convex, problem (2.6) for $\mu = 0$ admits only the trivial solution

$$(\rho_0, \kappa_0) := (1, 1). \quad (3.1)$$

This can be directly checked via Jensen's inequality by computing, for any $(\rho, \kappa) \in \mathcal{P} \times \mathcal{A}$,

$$E_0(\rho, \kappa) = \int_0^{2\pi} \Phi(\rho, \kappa) ds \stackrel{\text{Jensen}}{\geq} 2\pi \Phi\left(\frac{1}{2\pi} \int_0^{2\pi} \rho ds, \frac{1}{2\pi} \int_0^{2\pi} \kappa ds\right) = 2\pi \Phi(1, 1) = E_0(\rho_0, \kappa_0)$$

where the inequality is strict whenever ρ or κ are not constant, namely, whenever $(\rho, \kappa) \neq (\rho_0, \kappa_0)$. Let us mention that the integrand Φ is strictly convex if and only if

$$\beta'' > 0 \quad \text{and} \quad \beta'' \beta > 2(\beta')^2. \quad (3.2)$$

In order to allow the complex geometrical patterning of biological shapes to possibly be described by the minimization problem (2.6), one is hence forced to dispense of (3.2), for in that case the only minimizer of E_0 (and, a fortiori E_μ) would be the trivial one (ρ_0, κ_0) . In the setting of our bifurcation results, our choices for β will then fulfill

$$\beta''(\rho) \leq 0 \quad \text{or} \quad \beta''(\rho) \beta(\rho) \leq 2(\beta'(\rho))^2 \quad \text{for some } \rho \geq 0, \quad (3.3)$$

at least in a neighborhood of the trivial state ρ_0 .

On the other hand, lacking convexity of the integrand Φ , the energy E_0 fails to be weakly lower semicontinuous on $\mathcal{P} \times \mathcal{A}$, e.g. [14, Thm. 5.14], and existence of minimizers may genuinely fail. We collect a remark in this direction in the following.

Proposition 3.1 (No minimizers for E_0). *Assume that*

$$\beta(0) < \beta(\rho) \quad \forall \rho > 0. \quad (3.4)$$

Then, the minimization problem (2.6) with $\mu = 0$ admits no solution.

Before moving to the proof, let us point out that condition (3.4) implies in particular that Φ is not convex. Indeed, if Φ were convex, one could take any $\rho > 0$ and $\lambda \in (0, 1)$ and compute

$$\begin{aligned} \frac{1}{2} \beta(\rho) \kappa_0^2 &= \lim_{\lambda \rightarrow 1} \Phi(\lambda(0, \kappa_0/\lambda) + (1-\lambda)(\rho/(1-\lambda), 0)) \\ &\leq \lim_{\lambda \rightarrow 1} \left(\lambda \Phi(0, \kappa_0/\lambda) + (1-\lambda) \Phi(\rho/(1-\lambda), 0) \right) = \lim_{\lambda \rightarrow 1} \lambda \Phi(0, \kappa_0/\lambda) = \frac{1}{2} \beta(0) \kappa_0^2, \end{aligned}$$

contradicting (3.4). Note that the role of the value κ_0 in the latter computation is immaterial as one can argue with any $\kappa \neq 0$.

Proof of Proposition 3.1. Let us show that E_0 cannot be minimized on $\mathcal{P} \times \mathcal{A}$. We firstly remark that

$$E_0(\rho, \kappa) \stackrel{(3.4)}{\geq} E_0(0, \kappa) \stackrel{\text{Jensen}}{\geq} E_0(0, \kappa_0) \quad \forall (\rho, \kappa) \in \mathcal{P} \times \mathcal{A}. \quad (3.5)$$

In fact, the first inequality is strict as soon as $\rho\kappa \neq 0$ almost everywhere while the second one is strict as soon as κ is not constantly equal to κ_0 (recall that $\beta(0) > 0$). For all $\lambda \in (0, 1)$, we now define

$$\rho_\lambda(s) = \begin{cases} 0 & \text{for } s \in [0, \lambda\pi] \\ \rho_0/(1-\lambda) & \text{for } s \in (\lambda\pi, \pi] \\ 0 & \text{for } s \in (\pi, (1+\lambda)\pi] \\ \rho_0/(1-\lambda) & \text{for } s \in ((1+\lambda)\pi, 2\pi], \end{cases} \quad \kappa_\lambda(s) = \begin{cases} \kappa_0/\lambda & \text{for } s \in [0, \lambda\pi] \\ 0 & \text{for } s \in (\lambda\pi, \pi] \\ \kappa_0/\lambda & \text{for } s \in (\pi, (1+\lambda)\pi] \\ 0 & \text{for } s \in ((1+\lambda)\pi, 2\pi]. \end{cases}$$

We now check that $(\rho_\lambda, \kappa_\lambda) \in \mathcal{P} \times \mathcal{A}$. Indeed,

$$\int_0^{2\pi} \rho_\lambda ds = 2\pi(1-\lambda) \frac{\rho_0}{1-\lambda} = 2\pi\rho_0 = 2\pi, \quad \int_0^{2\pi} \kappa_\lambda ds = 2\lambda\pi \frac{\kappa_0}{\lambda} = 2\pi\kappa_0 = 2\pi.$$

Moreover, by letting $K_\lambda(s) = \int_0^s \kappa_\lambda(r) dr$, namely,

$$K_\lambda(s) = \begin{cases} \kappa_0 s / \lambda & \text{for } s \in [0, \lambda\pi] \\ \kappa_0 \pi & \text{for } s \in (\lambda\pi, \pi] \\ \kappa_0(s - (1-\lambda)\pi) / \lambda & \text{for } s \in (\pi, (1+\lambda)\pi] \\ \kappa_0 2\pi & \text{for } s \in ((1+\lambda)\pi, 2\pi], \end{cases}$$

we can compute

$$\begin{aligned} \int_0^{2\pi} \cos\left(\int_0^s \kappa_\lambda(r) dr\right) ds &= \int_0^{2\pi} \cos(K_\lambda(s)) ds \\ &= \int_0^{\lambda\pi} \cos(\kappa_0 s / \lambda) ds + \int_{\lambda\pi}^{\pi} \cos(\kappa_0 \pi) ds + \int_{\pi}^{(1+\lambda)\pi} \cos(\kappa_0(s - (1-\lambda)\pi) / \lambda) ds + \int_{(1+\lambda)\pi}^{2\pi} \cos(2\kappa_0 \pi) ds \\ &= \frac{\lambda}{\kappa_0} \sin(\kappa_0 \pi) - \frac{\lambda}{\kappa_0} \sin 0 + \cos(\kappa_0 \pi)(1-\lambda)\pi + \frac{\lambda}{\kappa_0} \sin(2\kappa_0 \pi) - \frac{\lambda}{\kappa_0} \sin(\kappa_0 \pi) + \cos(2\kappa_0 \pi)(1-\lambda)\pi \\ &= \lambda \sin \pi - \lambda \sin 0 + (\cos \pi)(1-\lambda)\pi + \lambda \sin 2\pi - \lambda \sin \pi + (\cos 2\pi)(1-\lambda)\pi = 0, \end{aligned}$$

and analogously

$$\begin{aligned} \int_0^{2\pi} \sin\left(\int_0^s \kappa_\lambda(r) dr\right) ds &= \int_0^{2\pi} \sin(K_\lambda(s)) ds \\ &= -\lambda \cos \pi + \lambda \cos 0 + (\sin \pi)(1-\lambda)\pi - \lambda \cos 2\pi + \lambda \cos \pi + (\sin 2\pi)(1-\lambda)\pi = 0. \end{aligned}$$

The latter ensures in particular that $(\rho_\lambda, \kappa_\lambda) \in \mathcal{P} \times \mathcal{A}$.

Let us now compute

$$E_0(\rho_\lambda, \kappa_\lambda) = \lambda E_0(0, \kappa_0/\lambda) + (1-\lambda)E_0(\rho/(1-\lambda), 0) = \lambda E_0(0, \kappa_0/\lambda)$$

and note that $E_0(\rho_\lambda, \kappa_\lambda) \rightarrow E_0(0, \kappa_0)$ as $\lambda \rightarrow 1$. Owing to (3.5), this entails that $E_0(\rho_\lambda, \kappa_\lambda)$ is an infimizing sequence on $\mathcal{P} \times \mathcal{A}$. On the other hand, the value $E_0(0, \kappa_0)$ cannot be reached in $\mathcal{P} \times \mathcal{A}$. Indeed, assume by contradiction to have $(\rho, \kappa) \in \mathcal{P} \times \mathcal{A}$ with $E_0(\rho, \kappa) = E_0(0, \kappa_0)$. Recalling (3.5), we have that $\rho\kappa = 0$ almost everywhere and $\kappa = \kappa_0$. This entails that $\rho = 0$ almost everywhere so that necessarily $(\rho, \kappa) = (0, \kappa_0)$, which however does not belong to $\mathcal{P} \times \mathcal{A}$. \square

Despite the lack of lower semicontinuity and the possible nonexistence of minimizers of variational problems, in some cases information may still be retrieved by analyzing the structure of infimizing sequences, see [1]. This perspective seems however to be of little relevance here. Assume (ρ, κ) to be a minimizer of E_0 in $\mathcal{P} \times \mathcal{A}$ and let $(\rho_\#, \kappa_\#)$ denote its periodic extension to \mathbb{R} . Let the *fine-scaled* trajectories

$$\rho_n(s) = \rho_\#(ns), \quad \kappa_n(s) = \kappa_\#(ns) \quad \forall s \in [0, 2\pi]$$

be defined. One may check that $(\rho_n, \kappa_n) \in \mathcal{P} \times \mathcal{A}$ as well and that $E_0(\rho_n, \kappa_n) = E_0(\rho, \kappa)$, so that all (ρ_n, κ_n) are minimizers (infimizing, in particular). On the other hand, (ρ_n, κ_n) weakly converges to its mean (ρ_0, κ_0) . This shows that, the limiting behavior of infimizing sequences may deliver scant information, for we recover the trivial state.

These facts motivate our interest for focusing on the case $\mu > 0$ in the minimization problem (2.6). In contrast to the case $\mu = 0$ of Proposition 3.1, energy E_μ can be minimized in $\mathcal{P} \times \mathcal{A}$ for all $\mu > 0$.

Proposition 3.2 (Existence for $\mu > 0$). *Let $\mu > 0$. Then, the minimization problem (2.6) admits a solution.*

Proof. This is an immediate application of the Direct Method. Let $(\rho_n, \kappa_n) \in \mathcal{P} \times \mathcal{A}$ be an infimizing sequence for E_μ (such a sequence exists, for $E_\mu(\rho_0, \kappa_0) > -\infty$). We can assume with no loss of generality that $\sup E_\mu(\rho_n, \kappa_n) < \infty$. In particular, as $\beta \geq \beta_m > 0$ we have that ρ_n and κ_n are uniformly bounded in $H^1(\mathbb{T}_{2\pi})$ and in $L^2(\mathbb{T}_{2\pi})$, respectively. This implies, at least for a not relabeled subsequence, that $\rho_n \rightharpoonup \rho$ in $H^1(\mathbb{T}_{2\pi})$ hence strongly in $C(\mathbb{T}_{2\pi})$ and $\kappa_n \rightharpoonup \kappa$ in $L^2(\mathbb{T}_{2\pi})$. We can hence pass to the limit in the relations

$$\int_0^{2\pi} \rho_n \, ds = 2\pi, \quad \int_0^{2\pi} \begin{pmatrix} \cos \left(\int_0^s \kappa_n(t) dt \right) \\ \sin \left(\int_0^s \kappa_n(t) dt \right) \end{pmatrix} ds = \begin{pmatrix} 0 \\ 0 \end{pmatrix}, \quad \int_0^{2\pi} \kappa_n \, ds = 2\pi$$

and obtain that $(\rho, \kappa) \in \mathcal{P} \times \mathcal{A}$ as well. Moreover, $\beta(\rho_n) \rightarrow \beta(\rho)$ strongly in $C(\mathbb{T}_{2\pi})$ as β is locally Lipschitz continuous. This implies that $(\beta(\rho_n))^{1/2} \kappa_n \rightharpoonup (\beta(\rho))^{1/2} \kappa$ in $L^2(\mathbb{T}_{2\pi})$ and lower semicontinuity ensures that $E_\mu(\rho, \kappa) \leq \liminf_{n \rightarrow \infty} E_\mu(\rho_n, \kappa_n) = \inf E_\mu$, so that (ρ, κ) is a solution of problem (2.6). \square

The parameter μ is a datum of the problem and it is in particular related to the characteristic length scale at which ρ changes along the curve. If μ is chosen to be large compared with the length of the curve, the minimizer is again forced to be trivial. Let us make these heuristics precise in the following.

Proposition 3.3 (Trivial minimizer for μ large). *For μ large enough, the trivial state (ρ_0, θ_0) is the unique solution of the minimization problem (2.6).*

Proof. We structure the proof into two steps. In Step 1 we show that, for μ large, the trivial state $u_0 = (\rho_0, \theta_0)$ with $\rho_0 = 1$ and $\theta_0(s) = s$ is a strict minimizer in a neighborhood which is independent of μ . In Step 2, we prove that all minimizers converge to u_0 in the H^1 norm as $\mu \rightarrow \infty$. The combination of these two steps entails then that all minimizers necessarily coincide with u_0 for μ sufficiently large, for they are arbitrarily close to u_0 (Step 2) which is locally the unique minimizer (Step 1).

Step 1: The trivial state is a strict local minimizer. Let us check that, for μ large enough, the second variation $\delta^2 E_\mu(u_0)$ of $E_\mu = \frac{1}{2} \int_0^{2\pi} (\beta(\rho) \dot{\theta}^2 + \mu \dot{\rho}^2) ds$ is positive. Indeed, for the arbitrary directions $u_1 = (\rho_1, \theta_1)$ and $\tilde{u}_1 = (\tilde{\rho}_1, \tilde{\theta}_1)$, we can compute

$$\delta^2 E_\mu(u_0)(u_1, \tilde{u}_1) = \int_0^{2\pi} \left(\frac{1}{2} \beta''(\rho_0) \dot{\theta}_0^2 \rho_1 \tilde{\rho}_1 + \beta'(\rho_0) \dot{\theta}_0 (\dot{\theta}_1 \tilde{\rho}_1 + \rho_1 \dot{\tilde{\theta}}_1) + \beta(\rho_0) \dot{\theta}_1 \dot{\tilde{\theta}}_1 + \mu^2 \dot{\rho}_1 \dot{\tilde{\rho}}_1 \right) ds,$$

which is uniformly continuous around u_0 . In particular, with $\dot{\theta}_0 = 1$ and rearranging terms,

$$\delta^2 E_\mu(u_0)(u_1, u_1) = \int_0^{2\pi} \left(\mu \dot{\rho}_1^2 + \beta(\rho_0) \dot{\theta}_1^2 + 2\beta'(\rho_0) \rho_1 \dot{\theta}_1 + \frac{\beta''(\rho_0)}{2} \rho_1^2 \right) ds.$$

By integrating by parts and using the Cauchy-Schwarz inequality in the third term we get

$$\begin{aligned} \delta^2 E_\mu(u_0)(u_1, u_1) &\geq \mu \int_0^{2\pi} \dot{\rho}_1^2 \, ds + \beta(\rho_0) \int_0^{2\pi} \dot{\theta}_1^2 \, ds \\ &\quad - \left(\frac{4\beta'(\rho_0)^2}{C\beta(\rho_0)} \right)^{\frac{1}{2}} \|\dot{\rho}_1\|_{L^2(0,2\pi)} (C\beta(\rho_0))^{\frac{1}{2}} \|\dot{\theta}_1\|_{L^2(0,2\pi)} - \frac{|\beta''(\rho_0)|}{2} \int_0^{2\pi} \rho_1^2 \, ds, \end{aligned}$$

where C is the Poincaré constant on $(0, 2\pi)$. Using again Poincaré's inequality to bound the second and last term in the right-hand side above, and Young's inequality for the third term we are left with

$$\delta^2 E_\mu(u_0)(u_1, u_1) \geq \left(\mu - \frac{2\beta'(\rho_0)^2}{C\beta(\rho_0)} - \frac{|\beta''(\rho_0)|}{2C} \right) \int_0^{2\pi} \dot{\rho}_1^2 \, ds + \frac{\beta(\rho_0)}{2} \int_0^{2\pi} \dot{\theta}_1^2 \, ds,$$

which is positive for

$$\mu > \frac{2\beta'(\rho_0)^2}{C\beta(\rho_0)} + \frac{|\beta''(\rho_0)|}{2C}.$$

As $\delta^2 E_\mu(u_0)$ is positive, u_0 minimizes E_μ on some neighborhood $U_\mu \subset \mathcal{P} \times \mathcal{A}$ for $\mu \geq \mu_0$ and for some $\mu_0 > 0$. Since E_μ is increasing in μ and $E_\mu(u_0)$ does not depend on μ , U_μ may be taken to be increasing in μ as well. Thus, u_0 minimizes E_μ on U_{μ_0} for all $\mu \geq \mu_0$.

Step 2: Global minimizers converge to the trivial state. We next prove that, for any $\delta > 0$ there exists $\mu_c > 0$ such that for any $\mu > \mu_c$, any global minimizer (ρ, θ) of E_μ is such that

$$\|\rho - \rho_0\|_{L^2(0,2\pi)} + \|\theta - \theta_0\|_{L^2(0,2\pi)} \lesssim \|\dot{\rho}\|_{L^2(0,2\pi)} + \|\dot{\theta} - \dot{\theta}_0\|_{L^2(0,2\pi)} < \delta \quad (3.6)$$

where we use the sign \lesssim to indicate the implicit occurrence of a constant just depending on data. In fact, we have that

$$\begin{aligned} E_\mu(\rho_0, \theta_0) \geq E_\mu(\rho, \theta) &= \int_0^{2\pi} \left(\frac{1}{2}\beta(\rho)\dot{\theta}^2 + \frac{\mu}{2}\rho^2 \right) ds \\ &\geq \int_0^{2\pi} \left(\frac{1}{2}\beta_m\dot{\theta}^2 + \frac{\mu}{2}\rho^2 \right) ds \geq \int_0^{2\pi} \left(\frac{1}{2}\beta_m\dot{\theta}_0^2 + \frac{\mu}{2}\rho^2 \right) ds, \end{aligned} \quad (3.7)$$

since θ_0 minimizes the Dirichlet energy $\int_0^{2\pi} \dot{\theta}^2 ds$ under the conditions $\theta(0) = 0, \theta(2\pi) = 2\pi$. Since $E_\mu(\rho_0, \theta_0) = \frac{1}{2} \int_0^{2\pi} \beta(\rho_0)\dot{\theta}_0^2 = \pi\beta(\rho_0) < \infty$, both terms in the above right-hand side are bounded. We hence deduce that $\int_0^{2\pi} \dot{\theta}^2 ds$ is bounded uniformly in μ and $\int_0^{2\pi} \rho^2 ds = O(\mu^{-1}) = o(\mu^{-1/2})$, so that there exists $\mu_1 > 0$ such that for $\mu > \mu_1$ we have $\int_0^{2\pi} \rho^2 ds < \delta/2$. Now, $\rho \in \mathcal{P}$ implies $\int_0^{2\pi} (\rho - \rho_0) ds = 0$ and by the Poincaré inequality as well as the continuous embedding in $L^\infty(0, 2\pi)$,

$$\|\rho - \rho_0\|_{L^\infty(0,2\pi)} \lesssim \|\dot{\rho}\|_{L^2(0,2\pi)} = o(\mu^{-1/4}),$$

and, by the local Lipschitz continuity of β ,

$$\|\beta(\rho) - \beta(\rho_0)\|_{L^\infty(0,2\pi)} = o(\mu^{-1/4}).$$

This allows us to refine estimate (3.7) as follows:

$$E_\mu(\rho_0, \theta_0) \geq E_\mu(\rho, \theta) \geq \int_0^{2\pi} \left(\frac{1}{2}\beta(\rho_0)\dot{\theta}_0^2 + \frac{\mu}{2}\rho^2 \right) ds + o(\mu^{-1/4}) = E_\mu(\rho_0, \theta_0) + \frac{\mu}{2} \int_0^{2\pi} \rho^2 ds + o(\mu^{-1/4}),$$

from which we get $\lim_{\mu \rightarrow \infty} \mu \int_0^{2\pi} \rho^2 ds = 0$, and then

$$\lim_{\mu \rightarrow \infty} E_\mu(\rho, \theta) = \lim_{\mu \rightarrow \infty} \int_0^{2\pi} \frac{1}{2}\beta(\rho)\dot{\theta}^2 ds = E_\mu(\rho_0, \theta_0).$$

Finally, we control

$$\left| \int_0^{2\pi} \frac{1}{2}\beta(\rho)\dot{\theta}^2 ds - E_\mu(\rho_0, \theta_0) \right| = \left| \int_0^{2\pi} \frac{\beta(\rho_0)}{2}(\dot{\theta}^2 - \dot{\theta}_0^2) ds + o(\mu^{-1/4}) \right|,$$

so to prove that $\lim_{\mu \rightarrow \infty} \int_0^{2\pi} \dot{\theta}^2 ds = \lim_{\mu \rightarrow \infty} \int_0^{2\pi} \dot{\theta}_0^2 ds = 2\pi$. This is enough to conclude that

$$\lim_{\mu \rightarrow \infty} \|\dot{\theta} - \dot{\theta}_0\|_{L^2(0,2\pi)} = 0.$$

We can then choose μ_2 such that, for $\mu > \mu_2$, $\|\dot{\theta} - \dot{\theta}_0\|_{L^2(0,2\pi)} < \delta/2$ and set $\mu_c = \max\{\mu_1, \mu_2\}$ for which the second inequality in (3.6) holds. The first inequality follows from Poincaré's inequality. \square

We present now a symmetry result which will turn out useful later on, when interpreting the numerical findings.

Proposition 3.4 (Symmetry of E_μ). *If (ρ, θ) is a local minimizer of E_μ for β , then $(2\rho_0 - \rho, \theta)$ is a local minimizer of E_μ for $\tilde{\beta}$, defined as $\tilde{\beta}(\rho) = \beta(2\rho_0 - \rho)$.*

Proof. The integrand is unchanged by this transformation, so that the first and second variations of E_μ at (ρ, θ) and $(2\rho_0 - \rho, \theta)$ when considering respectively β and $\tilde{\beta}$ are identical. \square

4 Bifurcation analysis

By Proposition 3.3, the circle with constant density is the global minimizer of the energy E_μ (1.1) for large enough values of the diffusivity μ . In this section candidates for nontrivial minimizers are constructed by bifurcation from this trivial critical point with decreasing $\mu > 0$ as bifurcation parameter. The analysis will be based on the Euler-Lagrange equations of a suitable Lagrangian, incorporating the constraints of closedness of the curve and of given total mass. Additional auxiliary conditions will eliminate symmetries resulting from arbitrary positioning of the curve in the plane.

4.1 Euler-Lagrange equations

We introduce the Lagrange multipliers $(\lambda_x, \lambda_y) \in \mathbb{R}^2$ for the closedness constraint and $\lambda_M \in \mathbb{R}$ for the mass constraint (cf. the definitions (2.3) and (2.4) of admissible θ and ρ respectively), and define the Lagrangian

$$\mathcal{L}(\bar{u}) := \frac{1}{2} \int_0^{2\pi} (\beta(\rho)\dot{\theta}^2 + \mu\rho^2) ds + \int_0^{2\pi} (\lambda_x \cos \theta + \lambda_y \sin \theta + \lambda_M(\rho - 1)) ds ,$$

with $\bar{u} = (\rho, \theta, \lambda_x, \lambda_y, \lambda_M)$, where $\rho, \theta - s \in H^1(\mathbb{T}_{2\pi})$. Critical points of the energy subject to the constraints solve the *Euler-Lagrange equations*

$$\mu\ddot{\rho} - \frac{1}{2}\beta'(\rho)\dot{\theta}^2 = \lambda_M , \quad (4.1)$$

$$\frac{d}{ds} (\beta(\rho)\dot{\theta}) = -\lambda_x \sin \theta + \lambda_y \cos \theta , \quad (4.2)$$

along with the *boundary conditions*

$$\rho(2\pi) - \rho(0) = 0 , \quad \dot{\rho}(2\pi) - \dot{\rho}(0) = 0 , \quad \theta(0) = 0 , \quad \theta(2\pi) = 2\pi , \quad (4.3)$$

and mass and closedness *constraints*

$$\int_0^{2\pi} \rho ds = 2\pi , \quad \int_0^{2\pi} \begin{pmatrix} \cos \theta \\ \sin \theta \end{pmatrix} ds = \begin{pmatrix} 0 \\ 0 \end{pmatrix} , \quad (4.4)$$

respectively. For every solution, new solutions can be produced by arbitrary shifts in s . In order to eliminate this degree of freedom we add the condition

$$\rho(0) = 1 , \quad (4.5)$$

where we note that 1 is the average value of ρ by the mass constraint, which is assumed by every continuous solution. One symmetry remains: The problem is still invariant under the flip symmetry $s \leftrightarrow -s$ (with $\theta \leftrightarrow -\theta$, $\lambda_y \leftrightarrow -\lambda_y$).

The *trivial solution* \bar{u}_0 of (4.1)–(4.5) (and the minimizer for large enough μ) is the unit circle with constant density:

$$\theta_0(s) = s , \quad \rho_0(s) = 1 , \quad \lambda_{x0} = \lambda_{y0} = 0 , \quad \lambda_{M0} = -\frac{1}{2}\beta'(1) . \quad (4.6)$$

For the stiffness coefficient β we shall assume the following local behavior close to the trivial solution:

$$\beta(\rho) = 1 + m(\rho - 1) + h\frac{(\rho - 1)^2}{2} + O((\rho - 1)^5) \quad \text{as } \rho \rightarrow 1 . \quad (4.7)$$

The bifurcation behaviour will be characterized in terms of the Taylor coefficients $m, h \in \mathbb{R}$. The complexity of the bifurcation computations below have motivated the simplifying assumption that the third- and fourth-order coefficients vanish. Including these higher-order terms would only alter the sub-/supercritical nature of the bifurcation, but not the critical values for the parameter μ .

4.2 Linearization around the trivial state

In terms of a small correction $\bar{u}_1 := \bar{u} - \bar{u}_0$, the linearization of problem (4.1)–(4.5) reads (using (4.7))

$$\mu\ddot{\rho}_1(s) - m\dot{\theta}_1(s) - \frac{h}{2}\rho_1(s) - \lambda_{M1} = f(s) , \quad (4.8)$$

$$\frac{d}{ds} (\dot{\theta}_1(s) + m\rho_1(s)) + \lambda_{x1} \sin s - \lambda_{y1} \cos s = g(s) , \quad (4.9)$$

subject to the boundary conditions

$$\rho_1(2\pi) - \rho_1(0) = 0, \quad \dot{\rho}_1(2\pi) - \dot{\rho}_1(0) = 0, \quad \theta_1(0) = 0, \quad \theta_1(2\pi) = 0, \quad (4.10)$$

the constraints

$$\int_0^{2\pi} \rho_1(s) ds = 0, \quad \int_0^{2\pi} \begin{pmatrix} -\sin s \\ \cos s \end{pmatrix} \theta_1(s) ds = \begin{pmatrix} \alpha_x \\ \alpha_y \end{pmatrix}, \quad (4.11)$$

and the auxiliary condition

$$\rho_1(0) = 0. \quad (4.12)$$

The inhomogeneities $f(s), g(s), \alpha_x, \alpha_y$ can be interpreted as nonlinear corrections.

Proposition 4.1 (Solution of the homogeneous linearized system). *A nonzero solution of (4.8)–(4.12) with $f = g = \alpha_x = \alpha_y = 0, \mu > 0, m, h \in \mathbb{R}$, only exists in the following cases:*

Case 1: *There exists $j \in \mathbb{N}, j \geq 2$, such that $\mu = \mu_j(m, h) := \frac{1}{j^2} (m^2 - \frac{h}{2}) \neq -\frac{h}{2}$. The space of solutions is one-dimensional and given by*

$$\rho_1(s) = a_1 \sin(js), \quad \theta_1(s) = \frac{a_1 m}{j} (\cos(js) - 1), \quad \lambda_{x1} = \lambda_{y1} = \lambda_{M1} = 0, \quad a_1 \in \mathbb{R}. \quad (4.13)$$

Case 2: $\mu = \mu_1(h) := -\frac{h}{2} \neq \frac{1}{j^2} (m^2 - \frac{h}{2})$ for all $j \in \mathbb{N}, j \geq 2$. *The space of solutions is one-dimensional and given by*

$$\rho_1(s) = b_1 \sin s, \quad \theta_1(s) = 0, \quad \lambda_{x1} = \lambda_{M1} = 0, \quad \lambda_{y1} = b_1 m, \quad b_1 \in \mathbb{R}. \quad (4.14)$$

Case 3: *There exists $j \in \mathbb{N}, j \geq 2$, such that $\mu = \mu_j(m, h) = \mu_1(h)$. The space of solutions is two-dimensional and given by*

$$\rho_1(s) = a_1 \sin(js) + b_1 \sin s, \quad \theta_1(s) = \frac{a_1 m}{j} (\cos(js) - 1), \quad \lambda_{x1} = \lambda_{M1} = 0, \quad \lambda_{y1} = b_1 m, \quad a_1, b_1 \in \mathbb{R}.$$

Remark 4.2. 1. As expected, bifurcations only occur under the condition (see (3.3))

$$2m^2 - h = 2\beta'(1)^2 - \beta(1)\beta''(1) > 0.$$

2. For Case 1 solutions, the curvature correction $\kappa_1 = \dot{\theta}_1$ satisfies $\kappa_1 = -m\rho_1$. This means that the sign of $m = \beta'(1)$ decides if curvature maxima coincide with density maxima ($m < 0$) or with density minima ($m > 0$), which is not a surprising result. The condition $j \geq 2$ is a manifestation of the Four Vertex Theorem (see Section 2).
3. Case 2 solutions exhibit only one maximum and one minimum of the density without any effect on the circular shape of the curve. The numerical computations reported in Section 5 show, however, that these solutions initiate bifurcating branches strongly deviating from the circular shape far enough from the bifurcation point.
4. Whereas Cases 1 and 2 correspond to codimension-one bifurcations, Case 3 represents a bifurcation of codimension two, whose nonlinear structure will not be analyzed in the following.
5. In a bifurcation scenario, where the values of m and h are fixed and the value of μ is decreased, there are several situations. For $h \geq 2m^2$ no bifurcations occur by convexity (see above). For $0 \leq h < 2m^2$ an infinite series of Case 1 bifurcations occurs at the bifurcation values $\mu_j, j \geq 2$, with the first one at $\mu = \mu_2$. For $h < 0$, apart from the bifurcations at $\mu = \mu_2, \mu_3, \dots$, there is also a Case 2 bifurcation at $\mu = \mu_1$. There are two subcases concerning the question, which bifurcation occurs first, determined by the criterion

$$\mu_1 > \mu_2 \iff h < -\frac{2}{3}m^2.$$

Codimension-two bifurcations occur whenever $\mu_1 = \mu_j$, i.e. $h = -2m^2/(j^2 - 1)$ for some $j \geq 2$. These observations are illustrated in the (m, h) -plane in Figure 4.1.

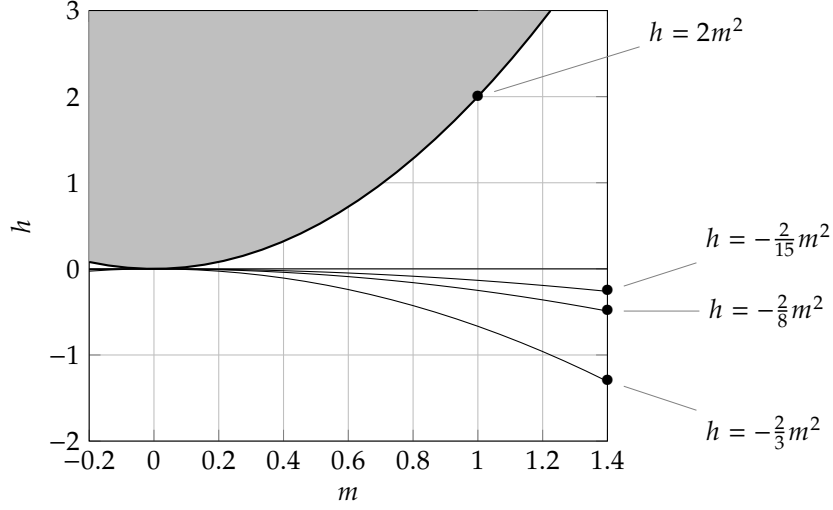


Figure 4.1: Regions of different bifurcation behaviour in the (m, h) -plane according to Proposition 4.1: No bifurcations above the parabola $h = 2m^2$. Only Case 1 bifurcations between the parabola and the m -axis. Case 1 and Case 2 bifurcations below the m axis, with codimension-two bifurcations on the parabolas $h = -2m^2/(j^2-1)$, $j \geq 2$. The first bifurcation is a Case 2 bifurcation below the parabola $h = -2m^2/3$, and a Case 1 bifurcation with $j = 2$ otherwise.

Proof. By the smoothness of solutions of ordinary differential equations we can employ Fourier representation and write

$$\rho_1(s) = \sum_{k \in \mathbb{Z}} \widehat{\rho}_{1,k} e^{iks}, \quad \theta_1(s) = \sum_{k \in \mathbb{Z}} \widehat{\theta}_{1,k} e^{iks}.$$

We keep the inhomogeneities for the moment, since this will be useful for the proof of the following result, and we use their Fourier series

$$f(s) = \sum_{k \in \mathbb{Z}} \widehat{f}_k e^{iks}, \quad g(s) = \sum_{k \in \mathbb{Z}} \widehat{g}_k e^{iks}.$$

The constraints (4.11) imply

$$\widehat{\rho}_{1,0} = 0, \quad \widehat{\theta}_{1,\pm 1} = \frac{1}{2\pi} (\alpha_y \pm i\alpha_x). \quad (4.15)$$

Comparing Fourier coefficients for $k = 0$ in (4.8), (4.9) implies

$$\lambda_{M1} = -\widehat{f}_0 \quad \text{and} \quad \widehat{g}_0 = 0, \quad (4.16)$$

where the latter has to be seen as a solvability condition for the inhomogeneous problem. Coefficients for $k = \pm 1$ in (4.8) and (4.9) give

$$-(\mu - \mu_1) \widehat{\rho}_{1,\pm 1} = \widehat{f}_{\pm 1} - \frac{m}{2\pi} (\alpha_x \mp i\alpha_y), \quad (4.17)$$

$$\pm m i \widehat{\rho}_{1,\pm 1} \mp \frac{i}{2} \lambda_{x1} - \frac{1}{2} \lambda_{y1} = \widehat{g}_{\pm 1} + \frac{1}{2\pi} (\alpha_y \pm i\alpha_x). \quad (4.18)$$

For coefficients with $|k| \geq 2$ we obtain

$$-\left(\mu k^2 + \frac{h}{2}\right) \widehat{\rho}_{1,k} - ikm \widehat{\theta}_{1,k} = \widehat{f}_k, \quad -k^2 \widehat{\theta}_{1,k} + ikm \widehat{\rho}_{1,k} = \widehat{g}_k,$$

implying

$$-k^2 (\mu - \mu_{|k|}) \widehat{\rho}_{1,k} = \widehat{f}_k - \frac{im}{k} \widehat{g}_k, \quad \widehat{\theta}_{1,k} - \frac{im}{k} \widehat{\rho}_{1,k} = -\frac{1}{k^2} \widehat{g}_k. \quad (4.19)$$

The results follow immediately from the homogeneous ($f = g = \alpha_x = \alpha_y = 0$) versions of (4.15)–(4.19), using the auxiliary conditions (4.12). \square

Lemma 4.3 (Solvability conditions). **Case 1:** Problem (4.8)–(4.12) with $0 < \mu = \mu_j \neq \mu_1$, $j \geq 2$, has a solution if and only if

$$j \int_0^{2\pi} f(s) \cos(js) ds = m \int_0^{2\pi} g(s) \sin(js) ds,$$

$$j \int_0^{2\pi} f(s) \sin(js) ds = -m \int_0^{2\pi} g(s) \cos(js) ds, \quad \text{and} \quad \int_0^{2\pi} g(s) ds = 0. \quad (4.20)$$

Case 2: Problem (4.8)–(4.12) with $0 < \mu = \mu_1 \neq \mu_j, \forall j \geq 2$, has a solution if and only if

$$\int_0^{2\pi} f(s) \cos s ds = m\alpha_x, \quad \int_0^{2\pi} f(s) \sin s ds = m\alpha_y, \quad \text{and} \quad \int_0^{2\pi} g(s) ds = 0. \quad (4.21)$$

Proof. For Case 1 the solvability conditions follow from (4.16), (4.19), and for Case 2 from (4.16), (4.17). \square

4.3 Asymptotic expansion around bifurcation points

For the codimension-one bifurcations identified above (Cases 1 and 2 in Proposition 4.1), the existence of bifurcating solution branches is guaranteed by general results on bifurcations from simple eigenvalues [8]. The local shape of these branches will be analyzed by perturbation expansions. By the presence of a flip symmetry in problem (4.1)–(4.5), pitchfork bifurcations can be expected, at least generically. For the bifurcation at $\mu = \mu_j, j \in \mathbb{N}$, we therefore introduce

$$\mu = \mu_j - \sigma A^2, \quad 0 < A \ll 1, \quad \sigma \in \{1, -1\}.$$

The small parameter A measures the distance from the bifurcation point, whereas the sign σ , to be determined by the analysis, tells us whether the bifurcation is *supercritical* for $\sigma > 0$ or *subcritical* for $\sigma < 0$. This convention is in line with the scenario of decreasing μ (see Remark 4.2, 5.). The solution $\bar{u} = (\rho, \theta, \lambda_x, \lambda_y, \lambda_M)$ of (4.1)–(4.5) will be approximated by an asymptotic expansion

$$\bar{u} = \bar{u}_0 + A\bar{u}_1 + A^2\bar{u}_2 + A^3\bar{u}_3 + O(A^4), \quad (4.22)$$

where the reason for going up to third order will become apparent below.

Remark 4.4 (Bifurcation diagram for classical elasticae). The expectation of pitchfork bifurcations and, thus, the ansatz (4.22) can also be motivated by the bifurcation diagram for classical elasticae (e.g. [20, Ch. 7]). The diagram shows an infinite series of bifurcations similar to the series of Case 1 bifurcations in (4.1)–(4.5). In the classical elastica problem all these bifurcations are supercritical pitchforks.

The notation in (4.22) is consistent with the above. The trivial rotationally symmetric solution of (4.1)–(4.5) is denoted by \bar{u}_0 , and the first correction \bar{u}_1 has to satisfy the homogeneous version ($f = g = \alpha_x = \alpha_y = 0$) of the linearized problem (4.8)–(4.12) with $\mu = \mu_j$, whose solution is unique up to a scalar constant (a_1 in Case 1 and b_1 in Case 2). The problems for \bar{u}_2 and \bar{u}_3 are determined by substituting the ansatz (4.22) into (4.1)–(4.5), expanding the nonlinearities and comparing coefficients of A^2 and A^3 . Both \bar{u}_2 and \bar{u}_3 solve inhomogeneous versions of the linearized problem (4.8)–(4.12) with $\mu = \mu_j$ and with the inhomogeneities

$$f_2 = \frac{m}{2} \dot{\theta}_1^2 + h\rho_1 \dot{\theta}_1, \quad g_2 = -\frac{d}{ds} \left(m\rho_1 \dot{\theta}_1 + \frac{h}{2} \rho_1^2 \right) - \theta_1 (\lambda_{x1} \cos s + \lambda_{y1} \sin s), \quad (4.23)$$

$$\begin{pmatrix} \alpha_{x2} \\ \alpha_{y2} \end{pmatrix} = \frac{1}{2} \int_0^{2\pi} \theta_1^2 \begin{pmatrix} \cos s \\ \sin s \end{pmatrix} ds, \quad (4.24)$$

for \bar{u}_2 , and

$$f_3 = \sigma \ddot{\rho}_1 + m\dot{\theta}_1 \dot{\theta}_2 + \frac{h}{2} (2\rho_2 \dot{\theta}_1 + 2\rho_1 \dot{\theta}_2 + \rho_1 \dot{\theta}_1^2), \quad (4.25)$$

$$g_3 = -\frac{d}{ds} \left(m\rho_1 \dot{\theta}_2 + m\rho_2 \dot{\theta}_1 + \frac{h}{2} \rho_1^2 \dot{\theta}_1 + h\rho_1 \rho_2 \right) - \theta_1 (\lambda_{x2} \cos s + \lambda_{y2} \sin s) - \theta_2 (\lambda_{x1} \cos s + \lambda_{y1} \sin s) + \frac{1}{2} \theta_1^2 (\lambda_{x1} \sin s - \lambda_{y1} \cos s), \quad (4.26)$$

$$\begin{pmatrix} \alpha_{x3} \\ \alpha_{y3} \end{pmatrix} = \int_0^{2\pi} \left(\theta_1 \theta_2 \begin{pmatrix} \cos s \\ \sin s \end{pmatrix} - \frac{1}{6} \theta_1^3 \begin{pmatrix} \sin s \\ \cos s \end{pmatrix} \right) ds, \quad (4.27)$$

for \bar{u}_3 . Note that the inhomogeneities depend on lower-order terms. So the terms in the asymptotic expansion (4.22) can be computed recursively. However, this comes with two problems, which are connected: the solution of the linearized problem is not unique (see Proposition 4.1), and it does not have a solution for arbitrary inhomogeneities (see Lemma 4.3). The strategy is to recover the lacking information for uniqueness from the solvability conditions for higher-order problems. It will turn out (as a consequence of the above mentioned flip

symmetry) that the inhomogeneities (4.23), (4.24) of the second-order problem satisfy the solvability conditions, no matter what the value of the missing first-order constant (a_1 in Case 1 and b_1 in Case 2) is. This is the reason why the third-order problem has to be considered, whose solvability condition will provide an equation for the missing first-order constant. In the following the essential results of these straightforward but lengthy computations will be given. They have been carried out manually and checked with the help of MATHEMATICA.

Case 1 bifurcations

The goal is to determine the value of the constant a_1 in the first-order correction \bar{u}_1 of the expansion (4.22), given in (4.13). The first step is the computation of the second-order terms.

Lemma 4.5 (Case 1: second-order solution). *Let $j \geq 2$ and \bar{u}_1 be given by (4.13). Then every solution of (4.8)–(4.12) with $0 < \mu = \mu_j \neq \mu_1$ and with the inhomogeneities given by (4.23), (4.24) can be written as*

$$\begin{aligned}\rho_2(s) &= a_2 \sin(js) + \frac{a_1^2(m(m^2 - h))}{2(2m^2 - h)}(\cos(2js) - \cos(js)), \\ \theta_2(s) &= a_2 \frac{m}{j}(\cos(js) - 1) - \frac{a_1^2(6m^4 - 6m^2h + h^2)}{8j(2m^2 - h)} \sin(2js), \quad a_2 \in \mathbb{R}, \\ \lambda_{x2} = \lambda_{y2} &= 0, \quad \lambda_{M2} = -\frac{a_1^2 m(m^2 - 2h)}{4}.\end{aligned}\tag{4.28}$$

Lemma 4.6 (Case 1: the missing constant). *Let $j \geq 2$, $0 < \mu_j \neq \mu_1$, and \bar{u}_1, \bar{u}_2 be given by (4.13), (4.28). Then the inhomogeneities given by (4.25)–(4.27) satisfy the solvability conditions (4.20), if and only if*

$$a_1 \left(j^2 \sigma - a_1^2 \frac{Z(m, h)}{8(2m^2 - h)} \right) = 0, \quad \text{with } Z(m, h) := -14m^6 + 36m^4h - 18m^2h^2 + h^3.\tag{4.29}$$

This shows that Case 1 bifurcations are pitchforks if and only if $Z(m, h) \neq 0$. The amplitude of the first-order term along the bifurcating branch is determined by the nontrivial solutions of (4.29):

$$a_1^2 = \frac{8j^2 \sigma (2m^2 - h)}{Z(m, h)},\tag{4.30}$$

which shows for the criticality $\sigma = \text{sign } Z(m, h)$ that the bifurcation is *supercritical* for $Z(m, h) > 0$ and *subcritical* for $Z(m, h) < 0$. Writing $Z(m, h) = m^6(z^3 - 18z^2 + 36z - 14)$ with $z := h/m^2 < 2$ shows that $Z(m, h) > 0$ and $2m^2 > h$ are equivalent to

$$z_1 < z < z_2 \quad \text{with } z_1 \approx 0.52 \quad \text{and } z_2 \approx 1.71.\tag{4.31}$$

Consequently, a supercritical pitchfork bifurcation occurs in the parabolic region $\{(m, h) \in \mathbb{R}^2 : z_1 m^2 < h < z_2 m^2\}$. Conversely, if (m, h) is such that $Z(m, h) < 0$, which holds for $h < z_1 m^2$ or $2m^2 > h > z_2 m^2$, then the bifurcation is subcritical. The situation is illustrated in Figure 4.2. Note that the criticality is independent from j . For a fixed pair (m, h) the whole series of Case 1 bifurcations has the same criticality.

Case 2 bifurcations

Lemma 4.7 (Case 2: second-order solution). *Let \bar{u}_1 be given by (4.14). Then every solution of (4.8)–(4.12) with $0 < \mu = \mu_1 \neq \mu_j, \forall j \geq 2$, and with the inhomogeneities given by (4.23), (4.24) can be written as*

$$\begin{aligned}\rho_2(s) &= b_2 \sin s + \frac{b_1^2 m h}{2(2m^2 + 3h)}(\cos(2s) - \cos s), \quad b_2 \in \mathbb{R}, \\ \theta_2(s) &= \frac{b_1^2 3h^2}{8(2m^2 + 3h)} \sin(2s), \\ \lambda_{x2} &= -\frac{b_1^2 m^2 h}{2(2m^2 + 3h)}, \quad \lambda_{y2} = b_2 m, \quad \lambda_{M2} = 0.\end{aligned}\tag{4.32}$$

Lemma 4.8 (Case 2: the missing constant). *Let $0 < \mu_1 \neq \mu_j, \forall j \geq 2$, and \bar{u}_1, \bar{u}_2 be given by (4.14), (4.32). Then the inhomogeneities given by (4.25)–(4.27) satisfy the solvability conditions (4.21), if and only if*

$$b_1 \left(\sigma + b_1^2 \frac{3h^3}{8(2m^2 + 3h)} \right) = 0.\tag{4.33}$$

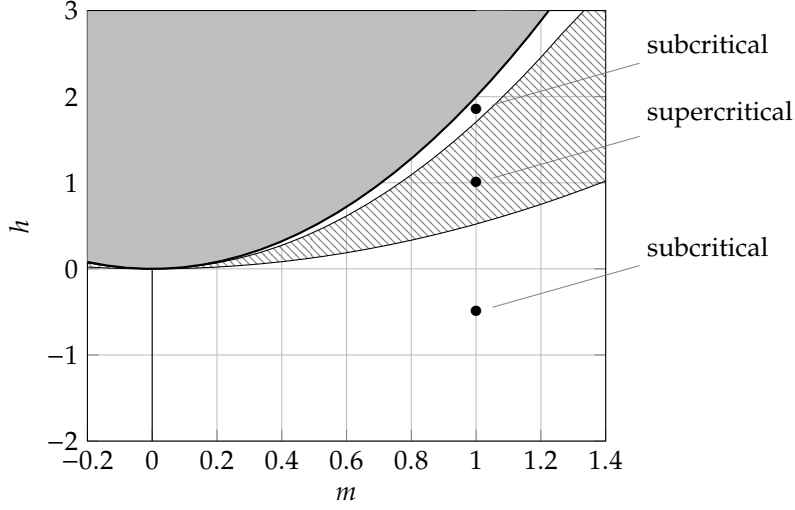


Figure 4.2: Contour plot of $Z(m, h)$ given by (4.29). The solution in Case 1 has the structure of a supercritical pitchfork bifurcation whenever $Z(m, h) > 0$ and $h < 2m^2$. These conditions define the crosshatched region $z_1 m^2 < h < z_2 m^2$ below the parabola $h = 2m^2$ (black line); $z_1 \approx 0.52$ and $z_2 \approx 1.71$, see (4.31). Conversely, if $Z(m, h) < 0$ which is true when $h < z_1 m^2$ or in the narrow white region given by $z_2 m^2 < h < 2m^2$, then the bifurcation is subcritical.

This shows that Case 2 bifurcations are pitchforks, since

$$b_1^2 = -\frac{8\sigma(2m^2 + 3h)}{3h^3}$$

is finite by $\mu_1 = -h/2 > 0$ and nonvanishing by $2m^2 + 3h = 8(\mu_2 - \mu_1) \neq 0$. The bifurcation is subcritical for $2m^2 + 3h < 0$, i.e. when the Case 2 bifurcation is the first one for decreasing μ (see Remark 4.2, 5.). It is supercritical for $2m^2 + 3h > 0$. It is also noteworthy that the circular shape of the trivial solution curve is now perturbed at the order of A^2 with the perturbation given in (4.32). The leading order density perturbation ρ_1 has both its extrema coinciding either with the maxima of the curvature perturbation $\dot{\theta}_2$ (in the subcritical case) or with its minima (in the supercritical case). This can be verified numerically, see Cases (iv) and (v) in Section 5.3 and Figure 5.4 for $j = 1$.

4.4 Energy and stability

As an indicator for the stability of bifurcating solutions, we investigate the changes of the energy (1.1) along bifurcating branches. For this purpose, we substitute $\mu = \mu_j - \sigma A^2$ and the asymptotic expansion (4.22) of the bifurcating solution into the energy and re-expand:

$$E_\mu(\rho, \theta) = \frac{1}{2} \int_0^{2\pi} (\beta(\rho) \dot{\theta}^2 + \mu \dot{\rho}^2) ds = E_0 + AE_1 + A^2E_2 + A^3E_3 + A^4E_4 + O(A^5).$$

For the coefficients we obtain (all computations of this section again verified with MATHEMATICA)

$$E_0 = \frac{1}{2} \int_0^{2\pi} ds = \pi = E_{\mu_j}(\rho_0, \theta_0), \quad E_1 = \frac{1}{2} \int_0^{2\pi} (m\rho_1 + 2\dot{\theta}_1) ds = 0, \quad (4.34)$$

$$E_2 = \frac{1}{2} \int_0^{2\pi} \left(2m\rho_1\dot{\theta}_1 + \frac{h}{2}\rho_1^2 + \dot{\theta}_1^2 + \mu_j\dot{\rho}_1^2 \right) ds, \quad (4.35)$$

$$E_3 = \frac{1}{2} \int_0^{2\pi} \left(2m\rho_1\dot{\theta}_2 + 2m\rho_2\dot{\theta}_1 + m\rho_1\dot{\theta}_1^2 + h\rho_1\rho_2 + h\rho_1^2\dot{\theta}_1 + 2\dot{\theta}_1\dot{\theta}_2 + 2\mu_j\dot{\rho}_1\dot{\rho}_2 \right) ds, \quad (4.36)$$

$$E_4 = \frac{1}{2} \int_0^{2\pi} \left(2m\rho_1\dot{\theta}_3 + 2m\rho_3\dot{\theta}_1 + m\rho_2\dot{\theta}_1^2 + 2m\rho_2\dot{\theta}_2 + 2m\rho_1\dot{\theta}_1\dot{\theta}_2 + \frac{h}{2}\rho_2^2 + h\rho_1\rho_3 \right. \\ \left. + 2h\rho_1\rho_2\dot{\theta}_1 + \frac{h}{2}\rho_1^2\dot{\theta}_1^2 + h\rho_1^2\dot{\theta}_2 + 2\dot{\theta}_1\dot{\theta}_3 + \dot{\theta}_2^2 + \mu_j\dot{\rho}_2^2 + 2\mu_j\dot{\rho}_1\dot{\rho}_3 - \sigma\dot{\rho}_1^2 \right) ds. \quad (4.37)$$

Lemma 4.9 (Energy expansion). *Let $j \in \mathbb{N}$, let \bar{u}_1, \bar{u}_2 be given by (4.13), (4.28) in Case 1, $j \geq 2$, or by (4.14), (4.32) in Case 2, $j = 1$. Let the constants a_1 in Case 1 or b_1 in Case 2 be chosen such that the third-order inhomogeneities (4.25)–(4.27) satisfy the solvability conditions of Lemma 4.6 in Case 1 and Lemma 4.8 in Case 2. Let \bar{u}_3 be a corresponding solution of the linearized problem (4.8)–(4.12) with $\mu = \mu_j$. Then the coefficients in the energy expansion above satisfy $E_1 = E_2 = E_3 = 0$ in both cases, as well as*

$$E_4 = -\frac{2\pi j^4(2m^2 - h)}{Z(m, h)} \quad (4.38)$$

in Case 1 with the notation of Lemma 4.6. In Case 2 we have

$$E_4 = \frac{2\pi(3h + 2m^2)}{3h^3}.$$

As expected, the sign of E_4 goes with criticality of the bifurcating branch. Stability is gained ($E_4 < 0$) along supercritical branches and lost ($E_4 > 0$) along subcritical branches. In particular, this can be expected to decide the stability of the branch corresponding to the first bifurcation for decreasing μ .

5 Numerical continuation of bifurcation branches

5.1 Discretization

The Euler-Lagrange equations (4.1) and (4.2) are discretized by finite differences as follows. For $N \in \mathbb{N}$ we discretize the interval $[0, L]$ by introducing $\Delta s = L(N-1)^{-1}$ and $s_i = i\Delta s$, $0 \leq i \leq N-1$, which naturally leads to the (abuse of) notation $\rho = (\rho_i)_{i=1}^{N-1}$, $\theta = (\theta_i)_{i=1}^{N-1}$ with $\rho_i = \rho(s_i)$, $\theta_i = \theta(s_i)$. This can be thought of as considering a polygonal approximation of the curve γ , where θ_i is the angle of the i^{th} side and where ρ_i is a piecewise constant approximation of ρ on that side (*i.e.* ρ_i is *not* associated to a vertex).

Using the notation $u = (\rho, \theta)$ and $\Lambda = (\lambda_x, \lambda_y, \lambda_M)$, we propose the following natural finite differences approximation for (4.1) and (4.2), respectively:

$$EL_\rho(u, \Lambda) = \mu \left(\frac{\rho_{i-1} - 2\rho_i + \rho_{i+1}}{\Delta s^2} \right) - \frac{1}{2}\beta'(\rho_i) \left(\frac{\rho_{i+1} - \rho_{i-1}}{2\Delta s} \right)^2 - \lambda_M = 0, \quad (5.1)$$

$$EL_\theta(u, \Lambda) = \frac{1}{\Delta s} \left(\beta \left(\frac{\rho_{i+1} + \rho_i}{2} \right) \left(\frac{\theta_{i+1} - \theta_i}{\Delta s} \right) - \beta \left(\frac{\rho_i + \rho_{i-1}}{2} \right) \left(\frac{\theta_i - \theta_{i-1}}{\Delta s} \right) \right) + \lambda_x \sin \theta_i - \lambda_y \cos \theta_i = 0, \quad (5.2)$$

for $0 \leq i \leq N-1$.

To remove the degree of freedom associated to solid rotations, we can set $\theta(0) = 0$ at the continuous level. This is reflected by the choice $\theta_0 = 0$ at the discrete level. We also need to provide values for indices $i = -1, N$. Again by periodicity we set $\rho_{-1} = \rho_{N-1}$, $\rho_N = \rho_0$, $\theta_{-1} = \theta_{N-1} - 2\pi$, and $\theta_N = \theta_0 + 2\pi$. Thus, we only consider (5.1) for $0 \leq i < N-1$ and (5.2) for $0 < i < N-1$.

The mass and closedness constraints can be naturally approximated as

$$C_M(u, \Lambda) = \Delta s \sum_{i=0}^{N-1} \rho_i - M = 0,$$

$$\begin{pmatrix} C_x \\ C_y \end{pmatrix} (u, \Lambda) = \Delta s \sum_{i=0}^{N-1} \begin{pmatrix} \cos \theta_i \\ \sin \theta_i \end{pmatrix} = 0.$$

We are left with a system of $2N + 1$ nonlinear equations which we propose to solve using a damped Newton method. If we assume $\bar{u}^k = (u^k, \Lambda^k)$ to be known, we look for \bar{u}^{k+1} as a solution to

$$J(\bar{u}^k)(\bar{u}^{k+1} - \bar{u}^k) = -\eta r(\bar{u}^k), \quad (5.3)$$

where $r(\bar{u}^k) = (EL_\rho, EL_\theta, C_x, C_y, C_M)$, J is the Jacobian of r with respect to \bar{u} , and $\eta \leq 1$ is the damping parameter with $\eta = 1$ corresponding to the standard Newton's method.

5.1.1 Continuation of branches

To follow numerically the bifurcation branches, one can pick some μ close to the critical value μ_j and take as initial value a perturbation of the trivial solution (corresponding to the circle with homogeneous ρ). The

position of μ relative to the critical value and the amplitude of the bifurcation are given precisely by the results of Section 4. Solving (5.3) yields a numerical approximation of a critical point, which can be used as initial condition for neighbouring values of μ . By iterating this process, one can move along the branch, provided that

1. the branch is locally smooth (for example, this is not the case when ρ hits zeros of β , where one could expect the branch to terminate),
2. the features of the solution can be resolved by the discretization with the chosen value of N .

5.2 Choice of parameters

In what follows we will consider a number of different situations, depending on the choice of parameters (m, h) for the function β , which will be of the form (4.7) with $\beta_0 = 1$, namely

$$\beta(\rho) = 1 + m(\rho - \rho_0) + \frac{h}{2}(\rho - \rho_0)^2.$$

As before we will take $M = L = 2\pi$, so that $\rho_0 = 1$. We consider six sets of parameters:

- (i) $(m, h) = (1, 1.85)$ corresponding to Case 1 with $\sigma = -1$ (subcritical bifurcation),
- (ii) $(m, h) = (1, 1)$ corresponding to Case 1 with $\sigma = 1$ (supercritical bifurcation),
- (iii) $(m, h) = (1, 1/4)$ corresponding to Case 1 with $\sigma = -1$ (subcritical bifurcation),
- (iv) $(m, h) = (1, -1/2)$ corresponding to Case 1 with $\sigma = -1$ (subcritical bifurcation) and supercritical Case 2,
- (v) $(m, h) = (1, -2)$ corresponding to Case 1 with $\sigma = -1$ (subcritical bifurcation) and subcritical Case 2,
- (vi) $(m, h) = (0, -1)$, which is similar to (v) in the special choice $m = 0$. At first order, γ should remain a circle, including for Case 1, as the correction coefficient $\theta_1 \equiv 0$ for $m = 0$, see (4.13).

For the definition of the different cases, we refer to Proposition 4.1. The parameters in (i) – (vi) are represented in Figure 5.1. The corresponding results are presented in Figures 5.3 and 5.4.

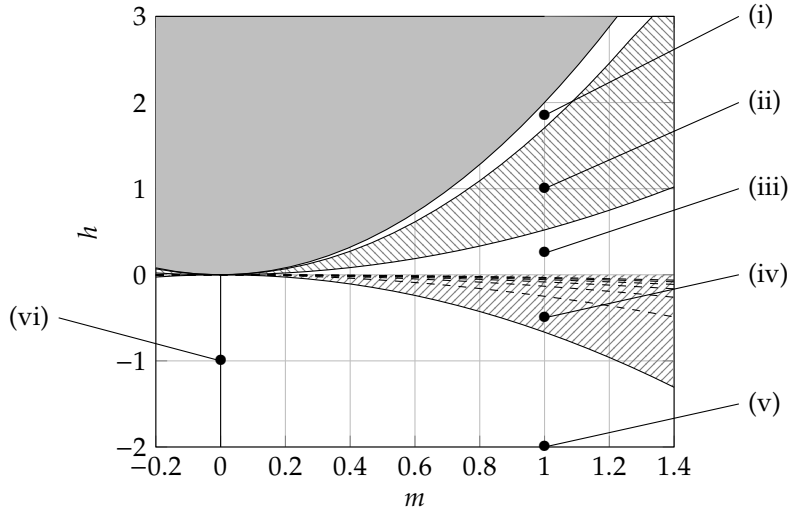


Figure 5.1: The different sets of model parameters (m, h) represented on the parameter space. The gray region corresponds to parameters which have no critical points except the trivial solution. The crosshatched region corresponds to supercritical bifurcations (Case 1 for $h > 0$, Case 2 for $h < 0$), and the plain white region to subcritical bifurcations. The dashed parabolas indicate where Case 3 occurs, for j up to 8.

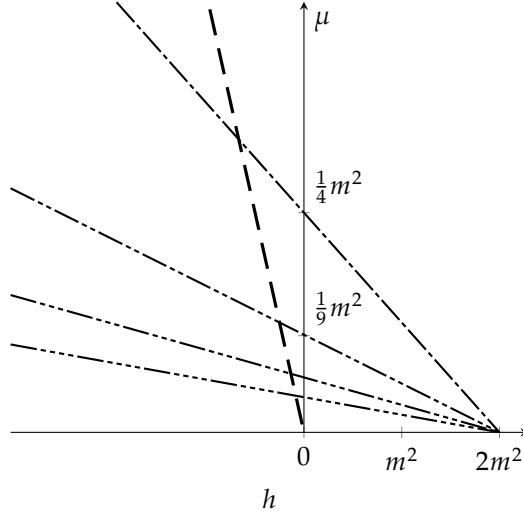


Figure 5.2: Critical values of μ for Case 1 (thin) and Case 2 (bold). The intersections correspond to (the degenerate) Case 3 which is not studied in this paper. The dashes indicate the value of j : — — for $j = 1$, - - - for $j = 2$, etc.

5.3 Results

The method described above (Section 5.1) was implemented in Julia [4]. Figure 5.3 presents the bifurcating branches both in terms of the amplitude of the density ρ and in terms of the energy E_μ . It offers a partial confirmation of the results of Section 4 in that:

- For Case (ii), $j \geq 2$ and (iv), $j = 1$, the bifurcation appears supercritical, i.e., the branch bifurcates to the left of the critical μ . Additionally, the energy decreases close to the trivial state. These branches offer critical points of E_μ which are candidates to be global minimizers.
- For all other cases, the bifurcation is subcritical, i.e., the branch bifurcates to the right of the critical μ , and the energy initially increases as one gets further from the trivial state.

Interestingly, Cases (i) and (iv) feature turning points, where the derivative of E_μ along the branch seems to change sign. In Case (i) it becomes negative, leading to critical points of lower energy with respect to the trivial state, and potentially global minimizers. This fact precludes uniqueness of minimizers of E_μ in general.

We were able to track an additional branch in Cases (i) to (iii), which seem to bifurcate from the $j = 2$ branch. No analytical results are available at this point, but we can make the following observations. The corresponding shapes, presented in gray in Figure 5.4, look like the ones obtained for $j = 1$ in Cases (iv) to (vi). This justifies the placement in the first column, although j has no meaning for this branch. In Cases (i) and (iii), it bifurcates from the $j = 2$ branch with decreasing energy for the choice of parameter considered. Case (ii) is a bit different, in that the bifurcation leads to critical points of higher energy, although the branch features a turning point, after which E_μ starts decreasing and eventually becomes smaller than for the $j = 2$ branch, for a given value of μ .

Other features of the critical points further along the branch can be seen in Figure 5.4. For Cases (i) to (v) and $j > 1$, one can identify the value of j with the number of flatter sections in each closed curve. These correspond to higher values of ρ , which agree with the fact that for all choices of parameters presented here, $m \geq 0$. This can be roughly thought as higher values of ρ penalizing higher values of the curvature $\hat{\theta}$. For $j = 1$ or in Case (vi), the situation is different, since the first-order correction $\theta_1 \equiv 0$. If one goes further in the expansion, one can expect that the next order correction θ_2 have the form $\cos(2js)$, that is half the period of ρ_1 . This could explain that in these cases, ρ seems to have j maxima when $\hat{\theta}$ has $2j$.

Additionally, far from the bifurcation point and after potential turning points, one can distinguish Cases (i) and (ii) from Cases (iii) to (vi). For the former, μ decreases along the branch, E_μ decreases and ρ seems to concentrate on flat sections. For the latter, the situation is the opposite: μ increases along the branch, E_μ increases and ρ stays rather smooth.

Remark 5.1. In Proposition 3.3 it is stated that for β bounded away from 0, only the trivial state (ρ_0, θ_0) is a minimizer of E_μ . The branches in Figure 5.3 which seem to continue far to large values of μ have an energy

clearly larger than $\pi = E_\mu(\rho_0, \theta_0)$. We also recall that for the results presented here, the choice of β is quadratic, and thus not bounded away from 0. There is then no contradiction of our analysis.

A systematic study of the stability in terms of the energy would be interesting, although probably necessarily limited to numerics, as it would help identifying local minimizers. Such an investigation is however out of the scope of this paper.

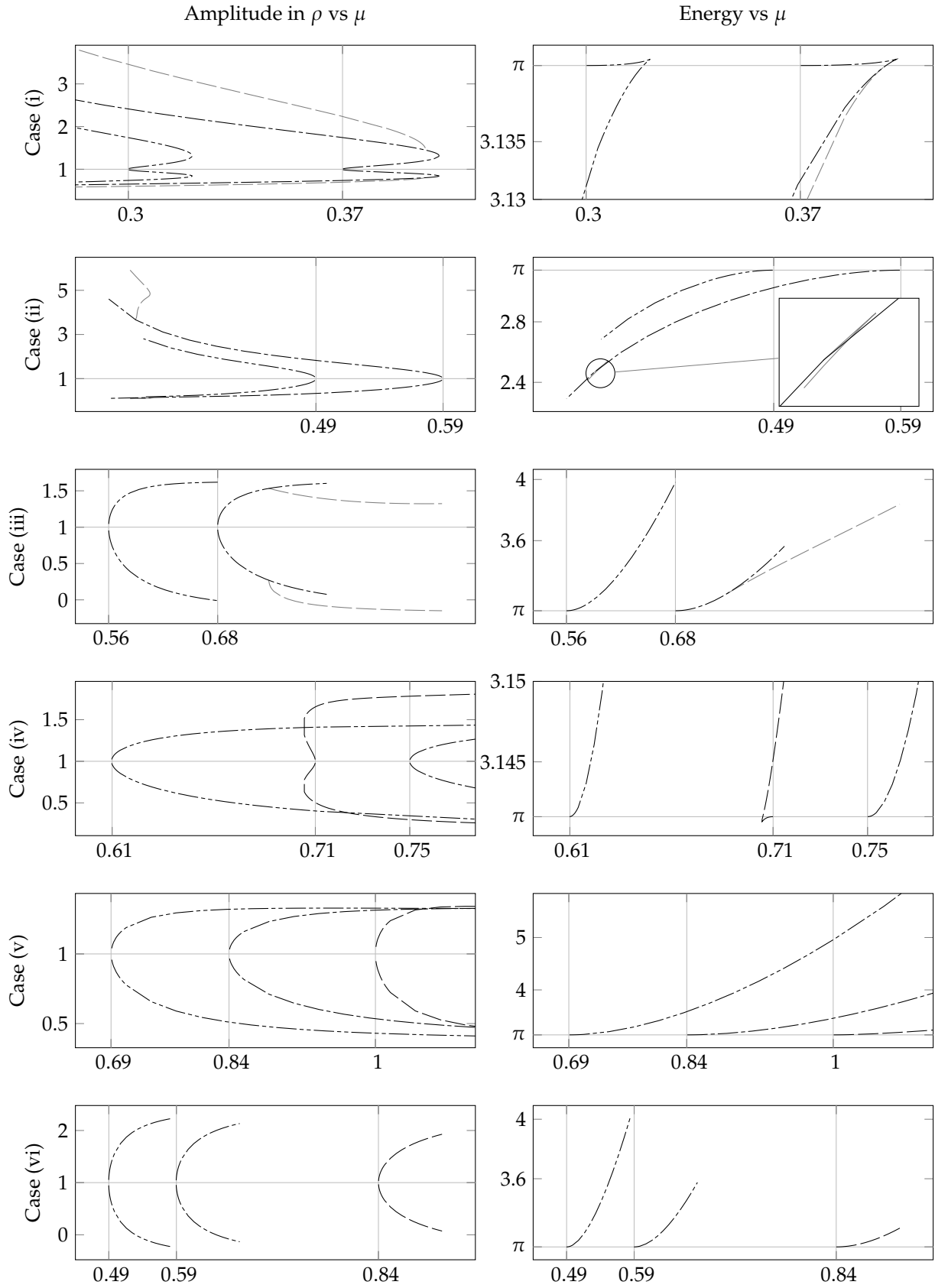


Figure 5.3: Numerical results for Cases (i) to (vi), in columns, for $j = 1, 2, 3$. The first column shows the amplitude in ρ , where the lower and greatest values of ρ are represented. The horizontal gray line corresponds to the trivial solution, for which $\rho \equiv 1$. The second column shows the energy E_μ , with the horizontal gray line again corresponding to the trivial solution, for which $E_\mu = \pi$. The dashes indicate the value of j for each branch: — for $j = 1$ (absent in (i) to (iii)), - - - for $j = 2$, - · - · for $j = 3$. The gray vertical lines indicate the theoretical critical values for μ . In Cases (i) to (iii), the secondary bifurcation branch is plotted in gray. As detailed in (4.22), at a supercritical (resp. subcritical) bifurcation point, the branch will appear for values of μ greater (resp. lower) than the critical value.

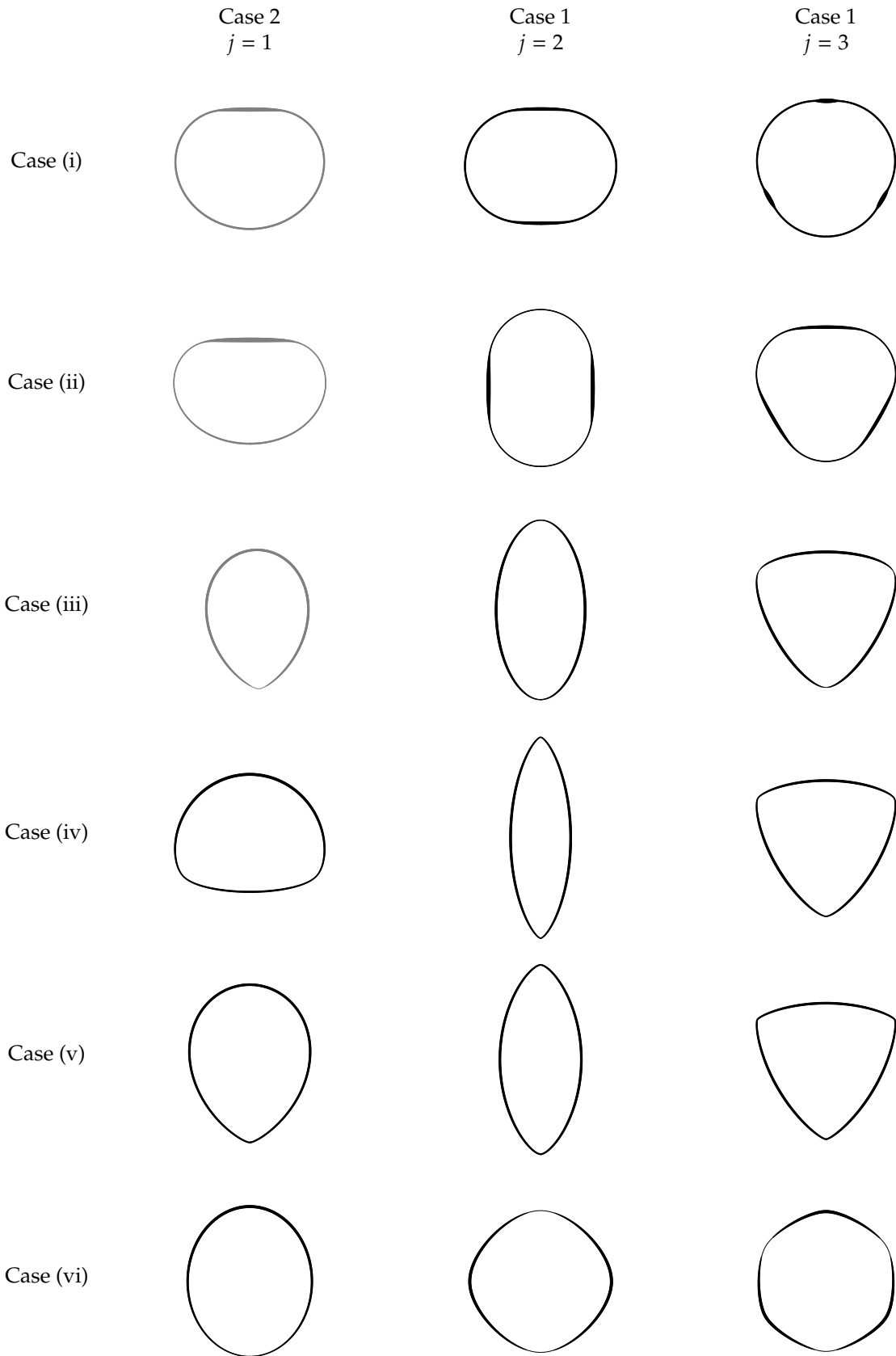


Figure 5.4: The shapes corresponding to each case, with $j = 1, 2, 3$ increasing with each column. These correspond to the last point computed on the branches shown in Figure 5.3. In Cases (i) to (iii), the shapes in the first column are in gray, as they do not correspond to branches bifurcating from the trivial state, and j is not defined in this case. They are placed in the first column due to their resemblance to shapes obtained for $h < 0$, in Cases (iv) to (vi). Thicker lines denote larger values of ρ .

6 Conclusion

To describe elastic curves in the plane, we introduced a regularized Canham-Helfrich type functional which includes a density-modulated stiffness β . We proved that the associated minimization problem has a solution if the regularization parameter is positive. If not, the problem has no solution in general. Conditions on the first derivatives of β were derived so that the problem has non trivial solutions. In this case, a bifurcation analysis around the trivial solution was performed, the regularization parameter playing the role of the bifurcation parameter. A family of both subcritical and supercritical pitchfork bifurcations were found, depending on the choice of β . This contrasts with the classical elastic curves, which display supercritical bifurcations only. An expansion of the energy confirmed that subcritical (resp. supercritical) solutions correspond to a gain (resp. a loss) of energy compared to the trivial state. This analysis was completed by numerical continuation of the bifurcating branches, which confirmed the theoretical findings. Secondary bifurcations and turning points—found numerically—testify of the intricate mathematical structure of the model. In particular no uniqueness should be expected for the minimization problem, except for large regularization.

Acknowledgements

This work has been supported by the Austrian Science Fund (FWF) projects F 65, W 1245, P 32788, by the Vienna Science and Technology Fund (WWTF) through Project MA14-009, and by the Austrian Academy of Sciences via the New Frontier's grant NST 0001.

References

- [1] J. M. Ball and R. D. James. Fine phase mixtures as minimizers of energy. *Archive for Rational Mechanics and Analysis*, 100(1):13–52, 1987.
- [2] J. W. Barrett, H. Garcke, and R. Nürnberg. Gradient flow dynamics of two-phase biomembranes: sharp interface variational formulation and finite element approximation. *SMAI J. Comput. Math.*, 4:151–195, 2018.
- [3] T. Baumgart, S. T. Hess, and W. W. Webb. Imaging coexisting fluid domains in biomembrane models coupling curvature and line tension. *Nature*, 425(6960):821–824, Oct. 2003.
- [4] J. Bezanson, A. Edelman, S. Karpinski, and V. B. Shah. Julia: a fresh approach to numerical computing. *SIAM Review*, 59(1):65–98, 2017.
- [5] K. Brazda, L. Lussardi, and U. Stefanelli. Existence of varifold minimizers for the multiphase Canham-Helfrich functional. *Calculus of Variations and Partial Differential Equations*, 59(3):Paper No. 93, 26, 2020.
- [6] P. B. Canham. The minimum energy of bending as a possible explanation of the biconcave shape of the human red blood cell. *Journal of Theoretical Biology*, 26(1):61 – 81, 1970.
- [7] R. Choksi, M. Morandotti, and M. Veneroni. Global minimizers for axisymmetric multiphase membranes. *ESAIM. Control, Optimisation and Calculus of Variations*, 19(4):1014–1029, 2013.
- [8] M. G. Crandall and P. H. Rabinowitz. Bifurcation from simple eigenvalues. *J. Functional Analysis*, 8:321–340, 1971.
- [9] B. E. J. Dahlberg. The converse of the four vertex theorem. *Proceedings of the American Mathematical Society*, 133(7):2131–2135, 2005.
- [10] K. Deckelnick, M. Doemeland, and H.-C. Grunau. Boundary value problems for a special Helfrich functional for surfaces of revolution: existence and asymptotic behaviour. *Calc. Var. Partial Differential Equations*, 60(1):Paper No. 32, 31, 2021.
- [11] M. P. do Carmo. *Differential geometry of curves and surfaces*. Prentice-Hall, Inc., Englewood Cliffs, N.J., 1976.
- [12] S. Eichmann. Lower semicontinuity for the Helfrich problem. *Ann. Global Anal. Geom.*, 58(2):147–175, 2020.
- [13] C. M. Elliott and L. Hatcher. Domain formation via phase separation for spherical biomembranes with small deformations. *European J. Appl. Math.*, page 1–26, 2020.

- [14] I. Fonseca and G. Leoni. *Modern methods in the calculus of variations: L^p spaces*. Springer Monographs in Mathematics. Springer, New York, 2007.
- [15] W. Helfrich. Elastic Properties of Lipid Bilayers: Theory and Possible Experiments. *Zeitschrift für Naturforschung C*, 28(11-12):693–703, Dec. 1973.
- [16] M. Helmers. Snapping elastic curves as a one-dimensional analogue of two-component lipid bilayers. *Mathematical Models and Methods in Applied Sciences*, 21(5):1027–1042, 2011.
- [17] M. Helmers. Convergence of an approximation for rotationally symmetric two-phase lipid bilayer membranes. *The Quarterly Journal of Mathematics*, 66(1):143–170, 2015.
- [18] J. Langer and D. A. Singer. Curve straightening and a minimax argument for closed elastic curves. *Topology. An International Journal of Mathematics*, 24(1):75–88, 1985.
- [19] L. Lussardi. The Canham-Helfrich model for the elasticity of biomembranes as a limit of mesoscopic energies. In I. M. Mladenov and V. Pulov, editors, *Proceedings of the XXI International Conference on Geometry, Integrability and Quantization, June 03–08, 2019, Varna, Bulgaria*, pages 1–11. Avangard Prima, Sofia, 2020.
- [20] J. E. Marsden and T. J. R. Hughes. *Mathematical foundations of elasticity*. Dover Publications, Inc., New York, 1994.
- [21] H. T. McMahon and J. L. Gallop. Membrane curvature and mechanisms of dynamic cell membrane remodelling. *Nature*, 438(7068):590–596, Dec. 2005.
- [22] A. Mondino and C. Scharrer. Existence and regularity of spheres minimising the Canham-Helfrich energy. *Arch. Ration. Mech. Anal.*, 236(3):1455–1485, 2020.
- [23] B. Palmer and Á. Pámpano. Anisotropic bending energies of curves. *Annals of Global Analysis and Geometry*, 57(2):257–287, 2020.
- [24] M. A. Peletier and M. Röger. Partial localization, lipid bilayers, and the elastica functional. *Arch. Ration. Mech. Anal.*, 193(3):475–537, 2009.
- [25] C. Truesdell. The influence of elasticity on analysis: the classic heritage. *Bull. Amer. Math. Soc. (N.S.)*, 9(3):293–310, 1983.
- [26] S. Wojtowytsch. Helfrich’s energy and constrained minimisation. *Commun. Math. Sci.*, 15(8):2373–2386, 2017.